Journal of Science and Transport Technology
Journal homepage: https://jstt.vn/index.php/en

Article info
Type of article:
Original research paper

DOI:
https://doi.org/10.58845/jstt.utt.2024.en.4.4.19-29

[*]**Corresponding author:**
Email address:
dungnttechnology@gmail.com

Received: 26/9/2024
Revised: 10/11/2024
Accepted: 21/11/2024

Impact of MoS_2 Layer Thickness and Donor Concentration on Saturation Current in 4-Layer MOSFET: A Comsol Simulation

Ştefan Ţălu[1], Dung Nguyen Trong[2,*], Umut Sarac[3], Luong Viet Trung[4], Mai Ho Thi Thanh[4], Huong Vuong Thi[4]

[1]Technical University of Cluj-Napoca, The Directorate of Research, Development and Innovation Management (DMCDI), 15 Constantin Daicoviciu St., Cluj-Napoca, 400020, Cluj county, Romania. E-mail: stefan.talu@auto.utcluj.ro, stefanta@yahoo.com

[2]University of Transport Technology, Faculty of Application Science, 54 Trieu Khuc, Thanh Xuan, Hanoi, Viet Nam. E-mail: dungnttechnology@gmail.com

[3]Bartın University, Department of Science Education, Bartın 74100, Turkey. E-mail: usarac@bartin.edu.tr

[4]University of Transport Technology, Faculty of Information Technology, 54 Trieu Khuc, Thanh Xuan, Hanoi, Viet Nam

Abstract: This study investigates the effects of the thickness and donor concentration of a hybrid MoS_2 semiconductor layer on the saturation current of a four-layer MOSFET, utilizing Comsol Multiphysics simulation software. By leveraging the software's capabilities to adjust physical parameters, we systematically analyze the influence of these variables on the device performance. Our findings indicate that increasing the MoS_2 layer thickness and donor concentration significantly enhances the saturation current, thereby improving the overall efficiency of the four-layer MOSFET. These simulation results align closely with experimental data and create a robust foundation for future studies and fabrication efforts aimed at optimizing the performance of MOSFETs through material engineering.

Keywords: Comsol Multiphysics, device efficiency, donor concentration, four-layer MOSFET, layer thickness, material engineering, MoS_2 semiconductor, saturation current.

1. Introduction

Molybdenum disulfide (MoS_2 hybrid) is a solid, black metallic powder characterized by a melting point (1422 K), a density (4.80 g/cm³ at 287 K), a purity (up to 99%), and particle sizes ranging from 150 to 1000 nm. MoS_2 hybrid functions as a semiconductor material, suitable for use in both single-layer and multi-layer structures [1]. Operating based on the field-effect transistor (FET) mechanism, it finds widespread application in various fields, including sensors, optoelectronic devices [2], and high-temperature applications due to its chemical stability [3]. It is extensively used in the production of displays [4], chemical sensors [5], optical detectors [6], integrated circuits [7], optoelectronic devices [8], biosensors [9], piezoelectric devices [10], and transistors [11]. Furthermore, MoS_2 hybrid is considered a promising next-generation semiconductor material thanks to its mechanical flexibility [12], optimal

band gap [13], high carrier mobility [14], and excellent transparency [15].

To study and fabricate hybrid MoS_2 materials, researchers predominantly employ both experimental and simulation-based approaches. The experimental techniques often involve chemical vapor deposition and physical vapor deposition methods to synthesize MoS_2 layers or nanotubes [16]. Experimental results have demonstrated that the band gap is affected by the MoS_2 nanotube diameter as well as the number of layers, with smaller diameters and fewer layers leading to a larger band gap [17]. For N-type MoS_2 semiconductors, the on/off current ratio has been observed to be approximately 60, and hybrid MoS_2 nanotubes exhibit favorable crystal structures and electrical properties, making them suitable for various electronic applications [18, 19].

In a related study, Dong et al. explored the phase transitions in doped ferroelectric polymers for MoS_2-based transistors, highlighting the potential for tunable electronic properties through donor concentration [20]. Additionally, Yoo et al. demonstrated that the physical properties of MoS_2-based electronic devices, particularly the contact resistance between the MoS_2 layers and the metal electrodes, are highly sensitive to the number of layers present [21]. This observation emphasizes the critical role of layer control in optimizing device performance. Furthermore, donor concentration subthreshold of metal oxides has proven to be an effective strategy for modulating the electronic properties of MoS_2, offering stability without decomposition [22]. However, it has been noted that the on/off current ratio tends to decrease at oscillation points when metal oxide donor concentration is employed [23].

In simulation approaches, researchers leverage Moore's law to predict and reduce the dimensions of MoS_2 materials, facilitating their application in next-generation nanoelectronic devices [24]. These simulations are often complemented by considerations of van der Waals forces, which have an important place in the assembly and behavior of 2D materials like MoS_2 [25]. Notably, hybrid MoS_2 materials possess tunable band gaps, making them highly versatile for use in nanoelectronic devices and further enabling their incorporation into a wide range of applications, from transistors to sensors [26].

To gain deeper insights into hybrid MoS_2 materials, it is important to examine the influence of electrical contact characteristics and the Schottky barrier in device performance [27]. The Schottky barrier, which forms at the metal-semiconductor interface, has a pivotal role in determining the efficiency of charge carrier injection, impacting the overall electrical behavior of MoS_2-based devices. Furthermore, the annealing process significantly affects the hysteresis behavior in MoS_2 devices, altering their stability and operational characteristics [28]. Annealing also has a profound impact on the contact mechanism between metal and semiconductor, optimizing the electrical contact and reducing contact resistance [29].

In general, MoS_2 has emerged as an optimal material for Metal-Oxide-Semiconductor Field-Effect Transistors (MOSFETs), which are crucial components in modern electronics. MOSFETs with MoS_2 are promising candidates for the miniaturization of electronic devices, particularly in applications requiring short channels, ultra-thin materials, and compact dimensions. These devices offer enhanced speed, high sensitivity, lightweight construction, and reduced power consumption, making them ideal for next-generation nanoelectronics [30]. Remarkably, MoS_2-based MOSFETs can be fabricated at sizes ranging down to the centimeter scale, further demonstrating their potential for integration in a wide range of applications [31].

In the current study, we proposed a robust model that examines the impact of both thickness and donor concentration of hybrid MoS_2 semiconductor material on the saturation current using COMSOL Multiphysics simulation software. The results obtained from the simulations show

excellent agreement with previous experimental data, providing a reliable foundation for future research and the fabrication of MOSFETs. The research results can be extended to 2D semiconductor materials. These findings are expected to be of considerable value to researchers working on the design and development of MoS_2-based devices.

2. Methodology

Initially, we selected the hybrid MoS_2 geometry for simulation within COMSOL Multiphysics software, as illustrated in Figure 1. This choice involved configuring the geometric parameters to accurately represent the four-layer hybrid MoS_2 structure.

Table 1 provides the detailed parameters used for modeling the hybrid MoS_2 in COMSOL Multiphysics. These parameters were meticulously chosen to ensure accurate modeling and simulation of hybrid MoS_2 materials, enabling precise analysis of their impact on device performance.

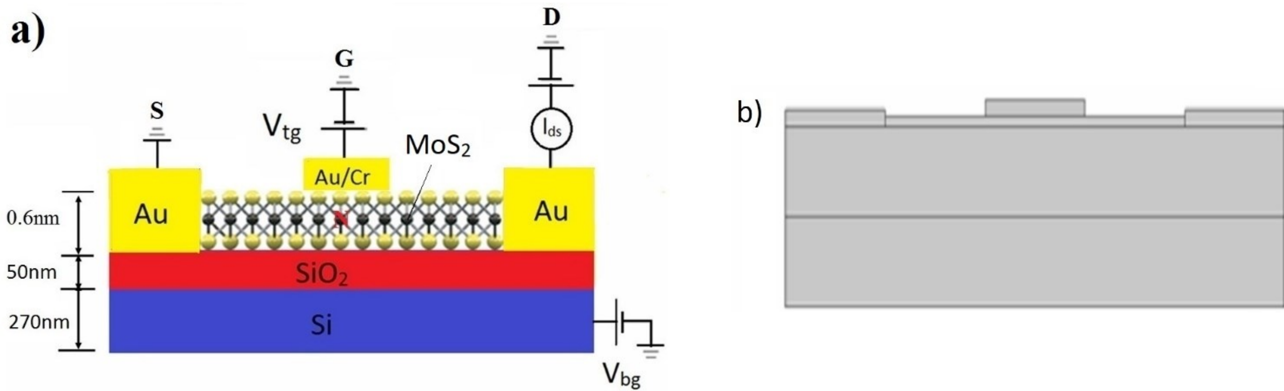

Figure 1. Geometry of MoS_2, including (a) the cross-section of a four-layer hybrid MoS_2 and (b) the model shape of hybrid MoS_2 in COMSOL Multiphysics

Table 1. Parameters of hybrid MoS_2

Parameters	Value	Parameters	Value
Thickness of MoS_2	0.6 nm/layer	Electron affinity 4L MoS_2	4 eV
Electron affinity 1L MoS_2	4.7 eV	Electron effective mass	0.5 m_0
Hole effective mass	0.5 m_0	Work function of gate	4.05 eV
Band gap 1L MoS_2	2.76 eV	Relative permittivity 1L	4.2
Band gap 4L MoS_2	1.6 eV	Relative permittivity 4L	11
SiO_2 thickness	300 nm	Thickness of gold contact	75 nm
Drain contact type	Ideal ohmic	Mobility 1L MoS_2	6 cm²/V·s
Shockley-Read-Hall (SRH) lifetimes 1L MoS_2	1.5 ns	Mobility 4L MoS_2	25 cm²/V·s
Shockley-Read-Hall (SRH) lifetimes 4L MoS_2	0.3 ns	Silicon thickness	2 µm
Length of MoS_2	3.5 µm	SiO_2 relative permittivity	3.9
Source contact type	Ideal ohmic	Width	6.8 µm

To determine the characteristic values of electron mobility in semiconductors, the Poisson equation is employed, reflecting how the charge density (ρ) influences the electric field within the material:

$$\nabla \cdot (\varepsilon \nabla V) = -\rho \quad (1)$$

where: ε represents the vacuum dielectric constant; V is the electric potential, and ρ denotes the charge density.

When evaluating semiconductor components, it is important to consider the contacts at the source, drain, and gate channels. The efficiency of these contacts, particularly those with Schottky interfaces, is quantified using the Richardson constant (A*) [32], described by equation:

$$A^* = \frac{4\pi q k_B^2 m^*}{h^3} \quad (2)$$

where: m*, h, k_B, and q show the effective mass of electrons or holes, Planck's constant, Boltzmann's constant, and charge, respectively. The Richardson constant is related to the thermal emission of carriers over the Schottky barrier, impacting the current-voltage characteristics of the device.

MoS_2 hybrid, made of Molybdenum and two atoms of Sulfur, and being an n-type doped semiconductor material, has a donor concentration (N_d) of 1×10^{18} cm^{-3}. This donor concentration influences the carrier concentration and overall electronic behavior of the material [33, 34].

Gauss's law for conservation of charge, that links the electric field to the charge distribution, is applied as follows:

$$D = \varepsilon \cdot E \quad (3)$$

where: D represents the electric displacement field, and E shows the electric field.

The charge present in the semiconductor quantifies the net charge distribution based on the carrier concentrations being described by [35]:

$$\rho^+ = q(p + N_d^+ - N_a^- - n); q = -e \quad (4)$$

N_d^+ shows the donor concentration, and N_a^- represents the acceptor concentration [35]. This equation quantifies the net charge distribution based on the carrier concentrations.

The gate (G) in the device, referred to as a recombination gate, includes contributions to the carrier current as modeled by the Shockley–Reed–Hall (SRH) recombination model. The SRH model specifically addresses non-radiative recombination, which occurs through defect states or impurity levels within the band gap of the semiconductor.

The SRH recombination rate for electrons (R_n) is given by [35]:

$$\frac{1}{\tau_n} = \frac{1}{\tau_{n0}} + \frac{p}{p_0} \quad (5)$$

where: $1/\tau_n$ is the total recombination rate of electrons; τ_{n0} is the intrinsic or baseline lifetime of electrons in the absence of any external influences; p represents the hole concentration in the semiconductor; and p_0 is the equilibrium hole concentration. The values of τ_n is influenced by material properties (such as the density of trap states, the quality of the crystal lattice, and the donor concentration levels).

Similarly, for holes (R_p), the recombination rate is given by [35, 36]:

$$\frac{1}{\tau_p} = \frac{1}{\tau_{p0}} + \frac{n}{n_0} \quad (6)$$

where: $1/\tau_p$ is the total recombination rate of holes; τ_{p0} is the intrinsic or baseline lifetime of holes; n is the electron concentration in the semiconductor; and n_0 is the equilibrium electron concentration. The values of τ_p are affected by the material's characteristics, including factors such as trap state density, crystal lattice quality, and donor concentration. The recombination rate, which significantly affects the carrier dynamics, depends on these lifetimes.

For this study, four layers of MoS_2 were modeled using the MAESTRO Macromodel [37]. Band gap values were extrapolated using density functional theory (DFT) combined with the extended Perdew–Burke–Ernzerhof (PBE) functional and a Gaussian-type orbital (GTO) basis set for geometry optimization. The MoS_2 model dimensions were set at 2.24nm × 2.24nm × 1.4nm with periodic boundary conditions (PBC) applied along the x and y axes, while the z-axis was excluded. To study the effect of thickness, two parameters such as number of layers and donor concentration must be kept constant to obtain accurate results.

The CLAYFF potential force field (as a

comprehensive tool used to model the interactions between atoms and molecules in a material system) was utilized to determine electrostatic interactions between atoms. After applying the CLAYFF force field [38], the analysis and visualization of the resulting atomic interactions and structures are carried out using specialized softwares: Visual Molecular Dynamics (VMD) [39] - a powerful tool for visualizing and analyzing molecular dynamics simulations; and Chimera – an advanced visualization tool used for molecular modeling that complements with VMD [40] software. Additionally, the methods used for characterizing and analyzing these nanostructures align with established techniques in the field [41] and are essential for accurate modeling and visualization of the material's electronic structure and interactions.

3. Results and discussion

A detailed analysis of the influence of the hybrid MoS_2 layer thickness and donor concentration on the electronic conductivity and performance of MOSFET devices, as modeled in Figure 2 and Figure 3 is given in this section.

3.1. Device configuration and parameters

Figure 2a illustrates the structure of the MOSFET device under study. The MOSFET consists of a silicon (Si) substrate with 270 nm thickness, covered by a silicon dioxide (SiO_2) insulating layer of 50 nm thickness. The Si layer, shown in blue, acts as the semiconductor base, while the SiO_2 layer, depicted in red, serves as the dielectric material. On top of this dielectric layer, we place the hybrid MoS_2 semiconductor material, consisting of four layers, and each 0.6 nm thick (Total thickness of these four layers is 2.4 nm). For each layer of MoS_2, the band gap is 2.76 eV, which reduces to 1.6 eV when aggregated to four layers. This hybrid MoS_2 functions as an N-type semiconductor.

The device features source (S) and drain (D) channels made of thin gold (Au) layers and a gate channel (G) composed of a gold-chromium alloy (Au/Cr) with yellow color, which acts as a P-type semiconductor. The contact surface area is optimized with an electrode channel width of 500 nm to minimize charge loss during electron transfer.

3.2. Electrical characteristics

Figure 2b demonstrates the correlation between the applied voltage (V_d) and the electron current intensity (I_d). For a hybrid MoS_2 layer with a thickness of 0.6 nm and a donor concentration of $N_d = 1\times10^{18}$ cm^{-3}, the current I_d increases linearly with voltage from 0 to 0.5 V. This linear relationship is due to the increasing electric field causing more electrons to migrate from the source to the drain. However, as V_d exceeds 0.5 V, the rate of increase in I_d begins to decelerate. This is attributed to the rising voltage increasing the electric field between the source and gate channels, leading to a portion of the electrons flowing through the gate channel, thus causing a slower increase in I_d. Further increases in donor concentration from 1×10^{18} to 2×10^{18} cm^{-3} result in a higher saturation current, rising from 3 to 8.13 μA, indicating improved conductivity with higher donor concentration levels.

3.3. Thickness and donor concentration effects

Figure 3a1 through 3a5 illustrates the impact of varying the hybrid MoS_2 layer thickness on the saturation current I_d according to donor concentration. The results show that increasing the donor concentration or increasing the thickness of a single MoS_2 layer increases the saturation current. These results are reflected in the electronic conductivity images shown in Figures 3b1 through 3b5. In which, dark blue represents low saturation current intensity and increases to green and highest is red.

For more details, the effect of MoS_2 layer thickness on the saturation current intensity is shown in Figure 4.

For a fixed donor concentration of N_d = 1×10^{18} cm^{-3}, increasing the MoS_2 layer thickness from 0.6 to 0.8 nm leads to an enhancement in the saturation current from 3.95 to 6.2 μA (Figure 4a). Similarly, for N_d = 1.5×10^{18} cm^{-3}, the current

increases from 8 to 13.5 μA (Figure 4b), and for $N_d = 2\times10^{18}$ cm^{-3}, it increases from 13.5 to 22 μA (Figure 4c).

The increased current with layer thickness and donor concentration is due to enhanced electronic conductivity. The thicker MoS_2 layers provide a greater volume for electron transport, while higher donor concentration increase the number of free charge carriers, both contributing to higher electron conductivity.

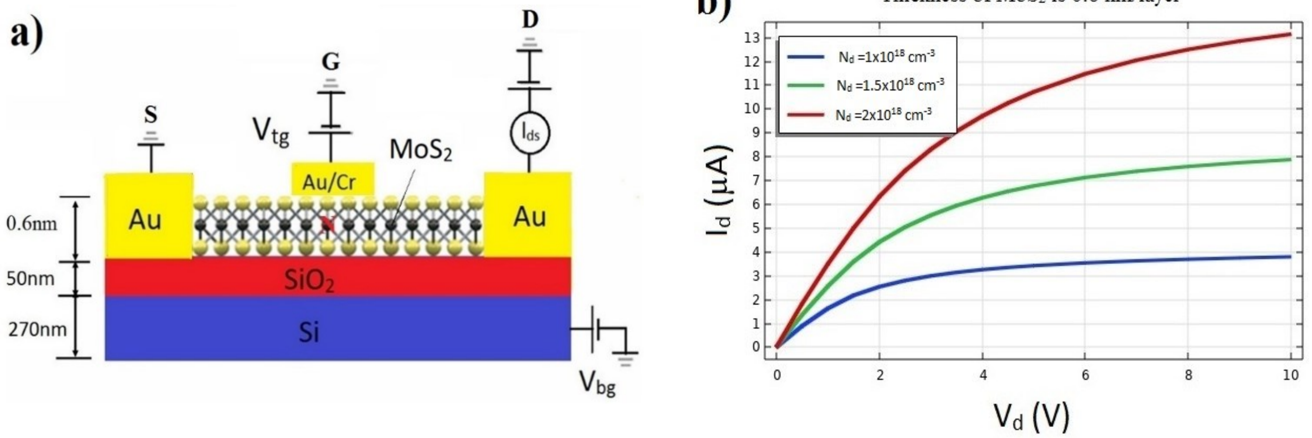

Figure 2. (a) Schematic representation of the MOSFET device structure and (b) Saturation current intensity for a MOSFET with a single 0.6 nm thick hybrid MoS_2 layer

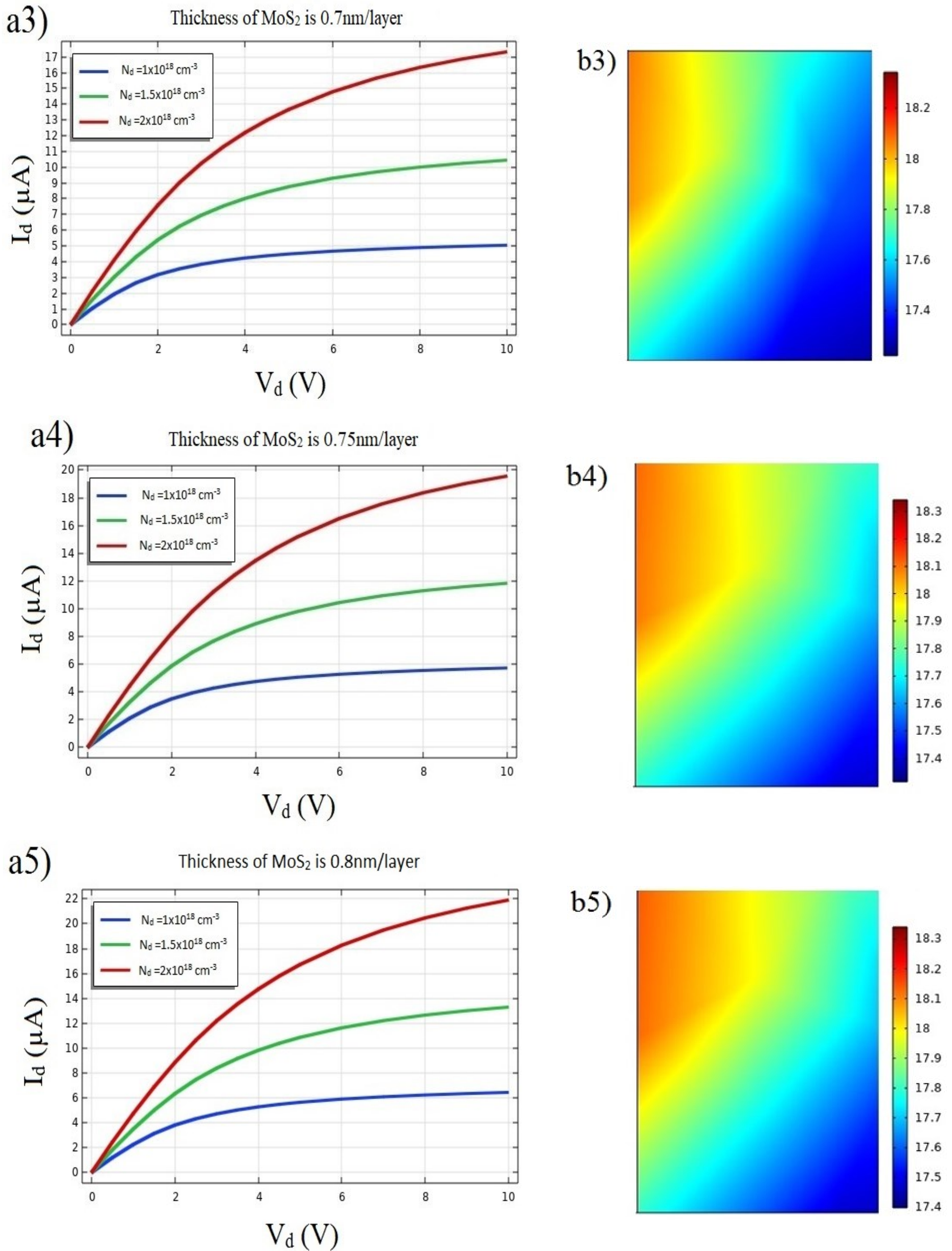

Figure 3. (a) Relationship between voltage and saturation current; (b) Electronic conductivity distribution across the MOSFET regions.

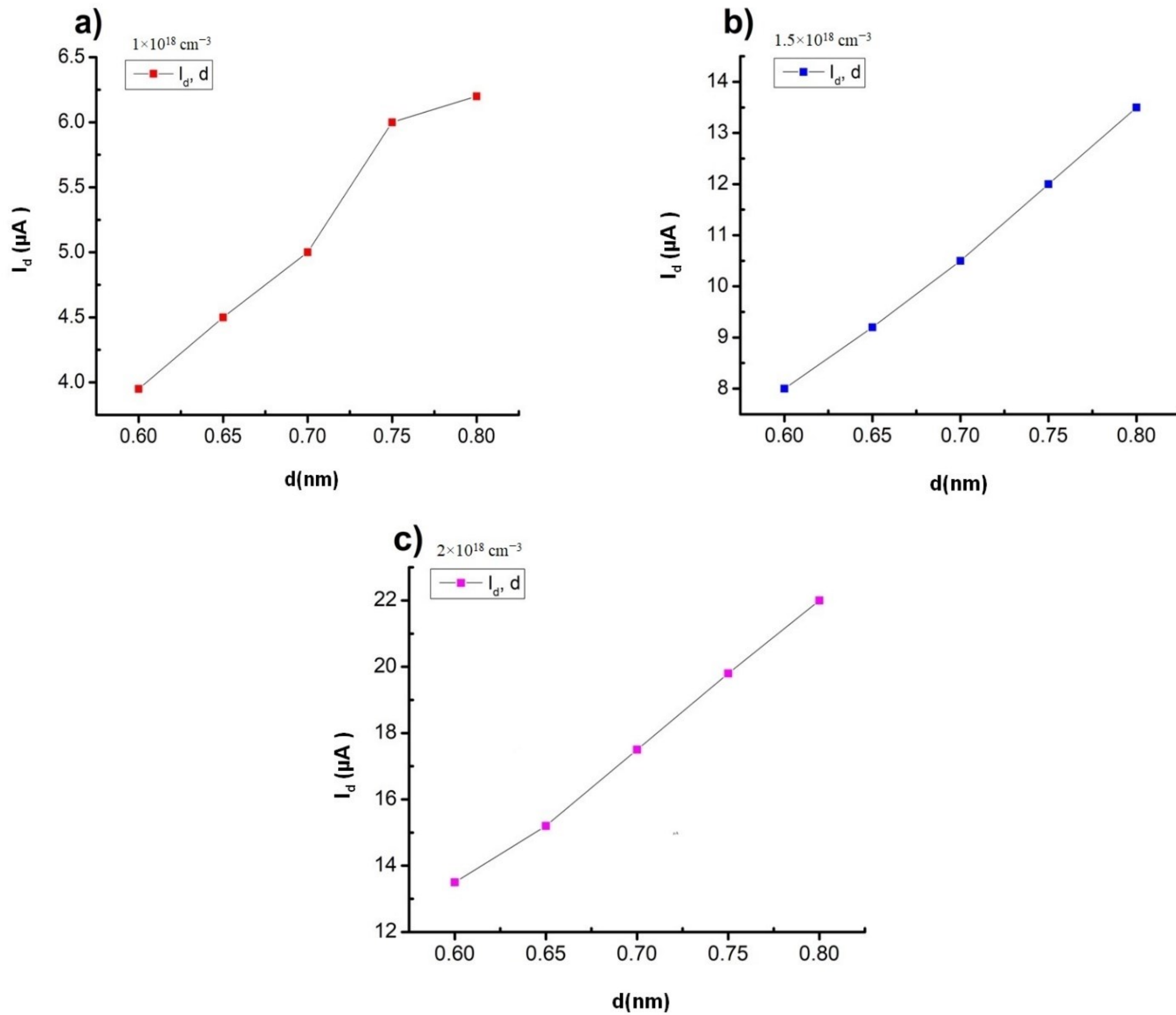

Figure 4. Relationship between I_d and thickness of MoS_2 layer

4. Conclusion

This research effectively investigates the impact of varying the hybrid MoS_2 semiconductor layer thickness and donor concentration on the saturation current intensity of a four-layer MOSFET, utilizing COMSOL Multiphysics software. The findings indicate that increasing the hybrid MoS_2 layer thickness from 0.6 to 0.65, 0.7, 0.75, and 0.8 nm results in a corresponding increasing in saturation current from 3.95 to 6.6 μA. This positive correlation suggests that the layer thickness significantly impacts charge carrier mobility and, consequently, the saturation current, as thicker MoS_2 layers may enhance the conductive pathways within the MOSFET, thereby facilitating a higher current flow. Furthermore, enhancing the donor concentration from 1×10^{18} to 1.5×10^{18} cm^{-3}, and 2×10^{18} cm^{-3}, significantly boosts the saturation current, demonstrating that both increased layer thickness and higher donor concentration levels improve MOSFET performance. In conclusion, this study provides a valuable foundation for future experimental studies aimed at developing advanced multilayer MOSFETs with enhanced efficiency and functionality.

Author Contributions: Ș.Ț.: writing original draft preparation and reviewing. D.N.T.: writing original draft preparation, conceptualization, software, investigation, resources, formal analysis, data curation, visualization, methodology, and supervision and reviewing. U.S., T.B., M.H.T.T., and H.V.T.: writing original draft preparation. All authors have read and agreed to the published

version of the manuscript.

ORCID and e-mails

Ştefan Ţălu, https://orcid.org/0000-0003-1311-7657. E-mails: stefan_ta@yahoo.com, stefan.talu@auto.utcluj.ro.

Dung Nguyen Trong, https://orcid.org/0000-0002-7706-1392. E-mail: dungnttechnology@gmail.com.

Umut Saraç, https://orcid.org/0000-0001-7657-173X. E-mail: usarac@bartin.edu.tr.

Funding: This research received no external funding.

Data Availability Statement: The data that support the findings of this study are available from the corresponding author upon reasonable request.

Competing interests: The authors declare that they have no competing interests.

References

[1] K.F. Mak, C. Lee, J. Hone, J. Shan, T.F. Heinz. (2010). Atomically thin MoS_2: A new direct-gap semiconductor. *Phys. Rev. Lett.*, 105(13), 136805.

[2] S. Barua, H.S. Dutta, S. Gogoi, R. Devi, R. Khan. (2018). Nanostructured MoS_2-based advanced biosensors: A review. *ACS Appl. Nano Mater.*, 1(1), 2–25.

[3] N. Bandaru, R.S. Kumar, D. Sneed, O. Tschauner, J. Baker, D. Antonio, S.N. Luo, T. Hartmann, Y. Zhao, R. Venkat. (2014). Effect of pressure and temperature on structural stability of MoS_2. *J. Phys. Chem. C*, 118(6), 3230–3235.

[4] S. Hwangbo, L. Hu, A.T. Hoang, J.Y. Choi, J.-H. Ahn. (2022). Wafer-scale monolithic integration of full-color micro-LED display using MoS_2 transistor. *Nat. Nanotechnol.*, 17(6), 500–506.

[5] R. Kumar, W. Zheng, X. Liu, J. Zhang, M. Kumar. (2020). MoS_2-based nanomaterials for room-temperature gas sensors. *Adv. Mater. Technol.*, 5(4), 1901062.

[6] W.J. Woo, E.K. Lee, H. Yoo, T. Kim. (2021). Unprecedentedly uniform, reliable, and centimeter-scale molybdenum disulfide negative differential resistance photodetectors. *ACS Appl. Mater. Interfaces*, 13(20), 25072–25081.

[7] Y. Zhou, J. Lu, Y. Hu, W. Wang, et al. (2022). High-performance MoS_2 complementary inverter prepared by oxygen plasma doping. *ACS Appl. Electron. Mater.*, 4(3), 955–963.

[8] S.K. Jain, M.X. Low, P.D. Taylor, S.A. Tawfik, M.J.S. Spencer, S. Kuriakose, A. Arash, C. Xu, S. Sriram, G. Gupta, et al. (2021). 2D/3D Hybrid of MoS_2/GaN for a high-performance broadband photodetector. *ACS Appl. Electron. Mater.*, 3(5), 2407–2414.

[9] Y. Zhang, D. Feng, Y. Xu, Z. Yin, W. Dou, U.E. Habiba, C. Pan, Z. Zhang, H. Mou, H. Deng, et al. (2021). DNA-based functionalization of two-dimensional MoS_2 FET biosensor for ultrasensitive detection of PSA. *Appl. Surf. Sci.*, 548, 149169.

[10] M. Dai, W. Zheng, X. Zhang, S. Wang, J. Lin, K. Li, Y. Hu, E. Sun, J. Zhang, Y. Qiu, et al. (2020). Enhanced piezoelectric effect derived from grain boundary in MoS_2 monolayers, *Nano Lett.*, 20(1), 201–207.

[11] Y. Jeong, H.J. Lee, J. Park, S. Lee, H.-J. Jin, S. Park, H. Cho, S. Hong, T. Kim, K. Kim, et al. (2022). Engineering $MoSe_2$/MoS_2 heterojunction traps in 2D transistors for multilevel memory, multiscale display, and synaptic functions. *npj 2D Mater. Appl.*, 6(1), 23.

[12] O. Samy, S. Zeng, M.D. Birowo, A. el Moutaouakil. (2021). A review on MoS_2 properties, synthesis, sensing applications, and challenges. *Crystals*, 11(3), 355.

[13] T. Kim, S. Fan, S. Lee, M.-K. Joo, Y.H. Lee. (2020). High-mobility junction field-effect transistor via graphene/ MoS_2 heterointerface. *Sci. Rep.*, 10(1), 13101.

[14] T. Shen, F. Li, L. Xu, Z. Zhang, F. Qiu, Z. Li, et al. (2020). High mobility monolayer MoS_2 transistors and its charge transport behavior under E-beam irradiation. *J. Mater. Sci.*, 55(21), 14315–14325.

[15] G.-H. Lee, Y.-J. Yu, X. Cui, N. Petrone, C.-H.

Lee, M.S. Choi, et al. (2013). Flexible and transparent MoS_2 field-effect transistors on hexagonal boron nitride-graphene heterostructures. *ACS Nano*, 7(9), 7931–7936.

[16] Y. Liu, F. Gu. (2021). A wafer-scale synthesis of monolayer MoS_2 and their field-effect transistors toward practical applications. *Nanoscale Adv.*, 3(6), 2117–2138.

[17] G. Seifert, H. Terrones, M. Terrones, G. Jungnickel, T. Frauenheim. (2000). Structure and electronic properties of MoS_2 nanotubes. *Phys. Rev. Lett.*, 85(6), 146–149.

[18] M. Strojnik, A. Kovic, A. Mrzel, J. Buh, J. Strle, D. Mihailovic. (2014). MoS_2 nanotube field effect transistors. *AIP Adv.*, 4(10), 107106.

[19] T. Okamoto, T. Shimizu, K. Takase, T. Ito, S. Shingubara. (2020). Formation of MoS_2 nanostructure arrays using anodic aluminum oxide template. *Micro Nano Eng.*, 9(1), 100–106.

[20] D.H. Lee, T. Park, T. Jeong, Y.K. Jung, J. Park, N. Joo, U. Won, H. Yoo. (2023). Dipole doping effect in MoS_2 field effect transistors based on phase transition of ferroelectric polymer dopant. *Front. Mater.*, 10, 1139954.

[21] H. Yoo, S. Hong, S. On, H. Ahn, H.-K. Lee, Y.K. Hong, et al. (2018). Chemical doping effects in multilayer MoS_2 and its application in complementary inverter. *ACS Appl. Mater. Interfaces*, 10(23), 23270–23276.

[22] W.J. Woo, S. Seo, T. Nam, Y. Kim, D. Kim, J.-G. Song, et al. (2021). MoS_2 doping by atomic layer deposition of high-k dielectrics using alcohol as process oxidants. *Appl. Surf. Sci.*, 541, 148504.

[23] C.J. McClellan, E. Yalon, K.K.H. Smithe, S. Suryavanshi, E. Pop. (2021). High current density in monolayer MoS_2 doped by AlO_x. *ACS Nano*, 15(2), 1587–1596.

[24] K. Andrews, A. Bowman, U. Rijal, P.-Y. Chen, Z. Zhou. (2020). Improved contacts and device performance in MoS_2 transistors using a 2D semiconductor interlayer. *ACS Nano*, 14(5), 6232–6241.

[25] H. Xu, H. Zhang, Z. Guo, P. Zhou, Y. Shan, S. Wu, et al. (2018). High-performance wafer-scale MoS_2 transistors toward practical application. *Small*, 14(48), 1803465.

[26] H. Nam, B.-R. Oh, P. Chen, M. Chen, S. Wi, W. Wan, et al. (2015). Multiple MoS_2 transistors for sensing molecule interaction kinetics, *Sci. Rep.*, 5(1), 10546.

[27] R. Yang, H. Li, K.K.H. Smithe, T.R. Kim, K. Okabe, E. Pop, et al. (2019). Ternary content-addressable memory with MoS_2 transistors for massively parallel data search. *Nat. Electron.*, 2(3), 108–114.

[28] C. Nie, B. Zhang, Y. Gao, M. Yin, X. Yi, C. Zhao, et al. (2020). Thickness-dependent enhancement of electronic mobility of MoS_2 transistors via surface functionalization. *J. Phys. Chem. C*, 124(31), 16943–16950.

[29] P. Bolshakov, P. Zhao, A. Azcatl, P.K. Hurley, R.M. Wallace, C.D. Young. (2017). Improvement in top-gate MoS_2 transistor performance due to high quality backside Al_2O_3 layer. *Appl. Phys. Lett.*, 111(3), 032110.

[30] P. Yang, X. Zou, Z. Zhang, M. Hong, J. Shi, S. Chen, J. Shu, L. Zhao, S. Jiang, X. Zhou, et al. (2018). Batch production of 6-inch uniform monolayer molybdenum disulfide catalyzed by sodium in glass. *Nat. Commun.*, 9(1), 979.

[31] F. Liu, W. Wu, Y. Bai, S.H. Chae, Q. Li, J. Wang, J. Hone, X.-Y. Zhu. (2020). Disassembling 2D van der Waals crystals into macroscopic monolayers and reassembling into artificial lattices. *Science*, 367(6482), 903–906.

[32] M. Shur. (1990). Physics of Semiconductor Devices. *Prentice Hall, Upper Saddle River, NJ, USA*.

[33] X. Li, H. Zhu. (2015). Two-dimensional MoS_2: Properties, preparation, and applications. *J. Mater.*, 1(1), 33–44.

[34] Y.H. Lee, X.Q. Zhang, W. Zhang, M.T. Chang, C.T. Lin, K.D. Chang, Y.C. Yu, J.T.W. Wang, C.S. Chang, L.J. Li, et al. (2012). Synthesis of large-area MoS_2 atomic layers with chemical

vapor deposition. *Adv. Mater.*, 24(17), 2320–2325.

[35] N. Pelagalli, E. Laudadio, P. Stipa, D. Mencarelli, L. Pierantoni. (2020). Efficient and versatile modeling of mono- and multi-layer MoS_2 field effect transistors. *Electronics*, 9(9), 1385.

[36] R.N. Hall. (1952). Electron-hole recombination in germanium. *Phys. Rev.*, 87(2), 387–388.

[37] A. Migalska-Zalas, I. Kityk, M. Bakasse, B. Sahraoui. (2008). Features of the alkynyl ruthenium chromophore with modified anionic subsystem UV absorption. *Spectrochim. Acta—Part A Mol. Biomol. Spectrosc.*, 69(1), 178–182.

[38] R. Cygan, J.J. Liang, A. Kalinichev. (2004). Molecular models of hydroxide, oxyhydroxide, and clay phases and the development of a general force field. *J. Phys. Chem. B*, 108(4), 1255–1266.

[39] C. Mayne, J. Saam, K. Schulten, E. Tajkhorshid, J. Gumbart. (2013). Rapid parameterization of small molecules using the force field toolkit. *J. Comput. Chem.*, 34(30), 2757–2770.

[40] E. Pettersen, T. Goddard, C. Huang, G. Couch, D. Greenblatt, E. Meng, T. Ferrin. (2004). UCSF Chimera - a visualization system for exploratory research and analysis. *J. Comput. Chem.*, 25(13), 1605–1612.

[41] Ș. Țălu. (2015). Micro and nanoscale characterization of three dimensional surfaces. Basics and applications. *Napoca Star Publishing House*. Cluj-Napoca, Romania.